Journal of Traffic and Transportation Engineering 5 (2017) 316-327
doi: 10.17265/2328-2142/2017.06.005

# Resolution Limits in Near-Distance Microwave Holographic Imaging for Safer and More Autonomous Vehicles

Dmitry Leshchiner[1], Konstantin Zvezdin[1], Grigory Chepkov[2], Pietro Perlo[3] and Anatoly Popkov[1]

*1. Moscow Institute of Physics and Technology, Moscow Region, 141707, Russian Federation;*

*2. Higher School of Economics, Moscow, 141707, Russian Federation;*

*3. IFEVS & Torino e-District, Torino, 12048, Italy*

**Highlights:** High sensitivity spin diodes as wave sensors are compact and cost effective devices for objects detection in different scenarios and weather conditions. Holographic reconstruction allows seeing the 3D density of the objects, indicating different materials—stone, flesh, metal, wood, etc. A computationally efficient holographic imaging and obstacle detection algorithm were targeted for use in a non-optical setting with a single coherent emitter and few detection sensors. The detection distances and spatial resolution proved sufficient for near-vehicle object detection purposes.

**Abstract:** We present a robust and computationally efficient image reconstruction and object detection algorithm suitable for a microwave holographic vision system with several microwave sensors and a single emission source to detect the presence and the nature of road obstacles impeding driving in the near vehicle zone. The holographic visualization technique allows reconstructing the spatial microwave scattering density in non-optical setting, detecting by lattice of sensors both amplitude and phase of a reflected signal. We discuss versions of an algorithm, determine and analyze its resolution limits for various distances with different number of sensors for a one-dimensional test problem of detecting two walls (or posts) separated by a gap at a fixed distance. The interval between sensors needed for a reliable reconstruction equals about one Fresnel zone width. We show that detection distances and spatial resolution achieved (better than 20 cm on distances up to 4.5 m) were sufficient for near-vehicle object detection purposes.

**Key words:** Spin diodes, microwave holography, image reconstruction, Tikhonov regularization, object detection.

## 1. Introduction

The growing interest in automated and connected vehicle technology prompted the need for efficient traffic and obstacle detection techniques in large variety of settings. To reach level 4 truly autonomous vehicles (Levels of Driving Automation, SAE International Standard J3016), the standard is putting emphasis on the automotive vision systems. Self-driving vehicles currently developed by Alphabet, Uber, or Toyota rely heavily on LIDAR (light detection and ranging). LIDAR can scan more than 100 m in all directions around the car, generating a precise 3D map of the surroundings. The main issues related to LIDAR in automotive industry are that they generate a large amount of data and that they are still too expensive for mass-market implementation. Much cheaper, in terms of price and computations, solutions are those based on radars and cameras. The cheapest and most available sensors are the cameras, the best for classification and texture interpretation. The cameras, however, use massive amounts of data, so processing becomes a computationally intense and algorithmically complex job. Radars are computationally much lighter than cameras and LIDAR. Radars can work in every weather condition and even use reflection to see behind obstacles; however, they are much less accurate than

**Corresponding author:** Leshchiner Dmitry Roaldovich, Ph.D., research fields: computer vision, data analysis, and pattern recognition. E-mail: dmitry_1111@inbox.ru.

LIDAR. Radar is a proven technology increasingly becoming more efficient for the autonomous car. The new RFCMOS (radio frequency complementary metal-oxide semiconductor) technology recently introduced to the market will allow smaller, lower power, efficient sensors that fit into the OEM (original equipment manufacturer) cost reduction strategies. This will also make radar more complementary to the cameras as the "dynamic duo" to "cross validate" the potential reconstructed scenario. Short-range 24 GHz and 77-79 GHz scanning radars work well for longer distance obstacle detection.

For safer inner-city mobility, as well as for vehicle parking setting, critical issues are control of obstacles and object movement in the near-vehicle zone, about 0.3 to 4.5 m distance to detection point. That would allow for speed control and adjustment in dense environment, vehicle-to-vehicle and pedestrian automatic emergency braking (with reaction time < 0.1 s) avoiding crashes and pedestrian fatalities at speeds less than 30 km/h, mitigating crashes in most inner-city environments [1].

Recently, there suggested an alternative approach to close-distance imaging [2] based on digital microwave holography, using high sensitivity spin diodes [3] as wave sensors. Those could provide compact and cost effective devices for dynamic detection of surrounding objects in different driving scenarios and weather conditions. Microwaves can penetrate various media—such as stone and water—so it can work at any weather, sense distant or inaccessible objects. Holographic reconstruction allows seeing the full 3D density of the objects—not just the object surface. Different densities indicate different materials—stone, flesh, metal, wood, etc.

At short distances, this technology combines the advantages of radars (work at every weather condition, low cost, can see behind obstacles) and of LIDAR (3D scenario reconstruction), adding also an extra capacity for object type detection, based on correct determination of object material. In this article, we discuss the potential of that technique for accurate obstacle recognition in near-vehicle zone from the image reconstruction and algorithmic point of view. We show that there exists a capacity to use it as a component in an integrated realistic object recognition automotive system.

## 2. The Technical and Algorithmic Setting for Near-Vehicle Object Detection Task

Digital holography techniques were first proposed in 1960s [4, 5] and extensively developed since [6-18]. They typically use a large array of sensors comparable in size to the object studied and a wide parallel imaging beam. In Ref. [19], authors explored a possibility to extend the holographic visualization diapason into the terahertz range by applying the high-resolution multi-spectral wave front registration. In Ref. [20], authors employed digital dark-field propagation for indoor Wi-Fi radiation imaging in the environment with multipath reflections. In our case, there is 3D picture where not only the waves scattering from various object volume points interfere, but also the object matter absorbs them on the way. There are microwave tomography techniques developed for medical purposes, addressing radiation absorption issues, based on nonlinear iterative inversion algorithms [21-24] and giving accurate information on the dielectric properties of the objects. In our application, however, there is no practical way to provide a parallel imaging beam comparable in size to the imaging field. We need to rely on just one or few compact radiation sources, emitting each within a certain angle. We also need to rely on just a few detection sensors here. Therefore, we deal with a radically non-optical setting. That has serious consequences for spatial resolution achievable. Indeed, looking at Fresnel zones size at the object edges, we would not normally expect spatial resolution much better than the half of the zone width. It remains unclear though even if that resolution is reliably achievable given the limited number of sensors

available for wave detection. As provided by Kotelnikov-Whittaker-Nyquist-Shannon sampling theorem [25-28], the maximal interval between sensors needed for a reliable reconstruction equals about Fresnel zone width. Same consideration implies that using more frequent sampling than that would not actually increase the amount of useful information available. With that in mind, we would realistically be looking at positioning no more than few dozens of sensors at the vehicle's front in order to reconstruct the image. Clearly, the 3D density map by size of a near-vehicle imaging field and with a resolution necessary for obstacle detection was controlled by at least couple of orders of magnitude more parameters than that. We will need effective parameters regularization techniques applied to reduce the dimensionality of the problem and still get the meaningful object detection results. We will present our approach below, together with an experimental analysis of the resolution achieved by that method at various detection distances and with various number of sensors used.

## 3. Image Reconstruction and Object Detection Algorithms Proposed

Here, we have the following setting. There is a 3D imaging field (a space zone) and a class of functions within that zone, representing a wave scattering density of objects, and represented by a finite-dimensional function space. As to the choice of a basis for density functions space, there could be number of representations, including, obviously, Fourier basis, but even a pixel-based density map would be a possibility. What is important is not a basis choice per se but the corresponding choice of space (e.g., using Fourier expansion with limited number of harmonics reduces the space dimensionality) and, most importantly, accompanying choice of regularization (expressing preferences for the shape of density solution). For instance, one could prefer smooth solutions or, alternatively, solutions with sharp density boundaries (which actually makes more sense for the obstacle detection task). One may prefer certain density values only (reflecting the expected physical properties of the object materials). One may also prefer that density be concentrated around certain areas of imaging field, focusing on object detection task within that area. In our paper here, we will work in Fourier basis. We will discuss the regularization effects below.

We will consider a task with one monochromatic radiation emitter, and several sensors. One could effortlessly extend the problem statement to cover various multiplexing schemes, several emission sources, etc., but we limit ourselves to the basic case; in particular, it is important since spin diodes are highly sensitive to a particular frequency so it is harder to use them in multiple frequency schemes. Given is the vector of $K$ sensor signals $P$ (these including both phase and amplitude) and the positions of both the emitter and the sensors. The article [1] gave the following expression for the scattered signal $P$ in terms of the functions expressing objects density in a point $\bar{r}$ within the imaging area, $f(\bar{r})$, and the emission intensity in direction to $\bar{r}$, $g(\bar{r})$:

$$P(p) = \int f(\bar{r}) \frac{g(\bar{r})}{R} e^{-i\omega R} d\bar{r}$$

where, $p$ is a position of a sensor, $\omega$ is signal frequency and $R$ is the length of the two-segment broken line from a position of the emitter $S$ to the point $\bar{r}$, and then to the $p$. That expression, however, takes no account of the signal adsorption within the object. Considering the adsorption intensity to be proportional to the scattering density (and normalizing the density function so that the proportionality coefficient equals to 1), the total adsorption coefficient is then given by $e^{-\oint_S^p f(\bar{x}) d\bar{x}}$, where, the integral in the exponent is taken along the same two-segment broken line from $S$ to $\bar{r}$ and then to the $p$, of the length $R$. Then we obtain a non-linear integral equation for the density function $f(\bar{r})$:

$$\int f(\bar{r}) \frac{g(\bar{r})}{R} e^{-\oint_S^p (f(\bar{x}) + i\omega) d\bar{x}} d\bar{r} = P(p)$$

What makes that equation non-linear is the adsorption term $e^{-\oint_S^p f(\bar{x})d\bar{x}}$. Still, if we assume a given density function, we may compute it, and fixing the term will now make the equation linear. It could then be solved numerically by linear algebra methods (keeping in mind that the functional space is finite-dimensional), and its solution will provide a correction to a previously given density. We may use that solution in its turn to obtain a newer correction, and so on.

We will discuss proper ways to solve the system, keeping in mind parameter regularization needs, in a moment. Let's note though that such scheme may work for a low dimension of density space—but talking about 3D Fourier expansion with 10 harmonics will give us $10^3$ = 1,000 parameters, and a function space of $N$ = 1,000 dimensions, and the need to invert a 1,000*1,000 matrix to obtain a solution—which is an $N^3$, i.e., $1{,}000^3 = 10^9$ computational cost. The inversion task becomes too costly to perform it in real time. The solution, however, may lie in ignoring the adsorption term altogether. Indeed, ignoring the term, we would still get accurate scattering picture of the front parts of the obstacles—the most critical ones to detect—and the image of distant parts slightly distorted by scattering adsorption. If we ignore the term, the task of inverting the matrix is still there, but the matrix no longer depends on the density function $f(\bar{r})$, and therefore its inversion could once and for all be precomputed. Moreover, what one needs to obtain the result is just a basis of density functions corresponding to each individual sensor. The result is simply a sum of these functions multiplied by each sensor's signal—a linear map from signal space to a density space. That gives us an easy and effective algorithm for object density reconstruction.

Let us present the formulae. To obtain a linear resolution procedure, one could present the regularization preferences as a quadratic weight within the functional space. The solution procedure (Tikhonov regularization [29-32]) is to find a solution with a minimal weight—or, more generally, a solution that minimizes the sum of a penalty for deviation from exact solution and of a regularization weight penalty. The weight is defined by a matrix $\Gamma$ and is given by $\|\Gamma f\|^2$, where $f$ is a proposed solution, $\|*\|$ is a standard (Euclidean or Hermitian) norm, and $\Gamma$ is a matrix that maps the vector $f$ into a norm space. The form for the total penalty is $\|Af - P\|^2 + \|\Gamma f\|^2$ where $P$ is the vector of sensor signals and $A$ is a matrix for linearized integral equation. Thus, the regularized solution given by $\tilde{f} = (A^T A + \Gamma^T \Gamma)^{-1} A^T P$ where $A^T$ and $\Gamma^T$ are Hermitian conjugate matrices to $A$ and $\Gamma$. So it is a result of multiplication of vector $P$ by a rectangular $N*K$ matrix $(A^T A + \Gamma^T \Gamma)^{-1} A^T$ which maps $K$-dimensional vector $P$ into $N$-dimensional vector $f$—or, in other words, a collection of $K$ basic functions $f_i, i = 1, \ldots, K$, each corresponding to its own sensor. Please note that it depends on sensor configuration only, so one may precompute this.

As stated above, the choice of a regularization matrix $\Gamma$ must reflect the preferences for a shape of the density solution. In the numerical experiments presented below, only one out of the whole variety of potential preferences has been explored—a preference for smoothness. The way to express it in Fourier basis is to define a diagonal matrix $\Gamma$ in which the diagonal term (the weight) depends on the number of a harmonics. Choosing the weight increasing with increase in harmonics number will enable a suppression of the high frequency noise. We found in numerical experiments that choosing the weight proportional to a harmonics number gives about the best performance.

Another way to reduce the dimensionality is to simplify the density functions. In particular, given that we only care about vehicle movement obstacles, we may largely ignore the height structure of the objects, confining ourselves to resolving the 2D (the width-depth) shape of the object within the given

height range corresponding to vehicle dimensions. In the next section, we give results of numerical experiments corresponding to a task of imaging and detecting a 1D object structure (a slot—two walls separated by a gap) at a given distance.

For that 1D task, we used a particular object detection algorithm. Namely, we assume that object density could only take two values 0 and 1 (all objects are of the same density—as in, of the same material) and we would like to distinguish between the two cases. The way to do it is to set a density threshold and assume zero density for all reconstructed density values below the threshold and density one for all the values above. Here is how we choose the threshold. We take the point lattice with a period equal to the wave length, take all the reconstructed values in these points, and put a threshold in the middle of the largest interval between the values (i.e., to the point of "lowest values density"—hopefully corresponding to the point between the cluster groups of high and low density values). Applying the chosen threshold to the reconstructed density, we then get back a reconstructed object shape. Having thus fixed the object detection procedure, we made a series of numerical experiments testing its resolution power with various object distances and configurations of sensors. Fig. 1 gives an illustration of how the algorithm worked for a particular case (32 sensors, object distance is 50 wavelengths).

## 4. Numerical Experiment Setting and Results

There was a series of experiments detecting the 1D slots (two walls divided by a gap) at a given distance conducted to determine the spatial resolution limits for the algorithm described above. Spatial resolution refers to the ability of the imaging to differentiate two objects. Low spatial resolution techniques will be unable to differentiate between two objects that are relatively close together. In our case, objects are the slot walls and the closeness of the objects is the width of the gap. We determine the gap resolution limits depending on the object distance and the configuration of walls, for several configuration of sensors. The imaging field size was fixed to be of 64 wavelengths (for a realistic case of spin diodes set to 10 GHz frequency, that would be about 2 m), and the size of sensors lattice was fixed to be the same (that would roughly correspond to a width dimension of a car). We assume the emitter was monochromatic, wide-beam, positioned at the center of

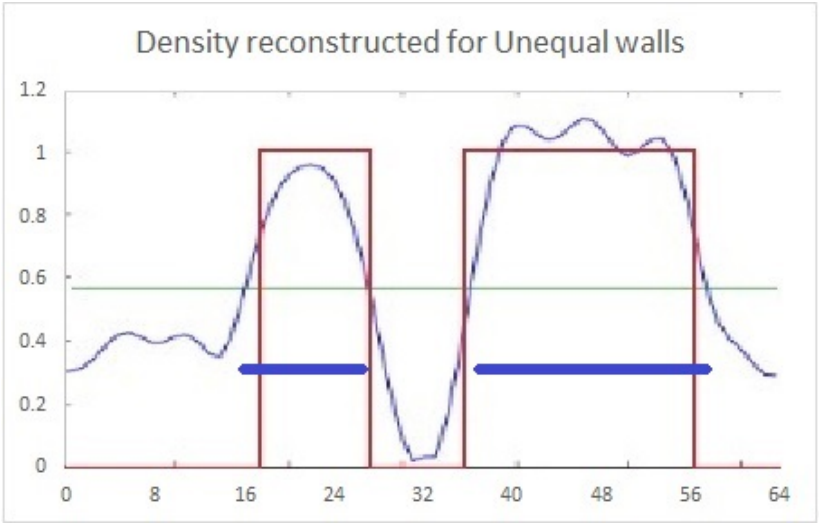


**Fig. 1 A reconstructed 1D density for a given slot shape (gap 8 wavelengths, smaller wall 10 wavelengths). X-axis is the object point coordinate measured in wavelength units ($x = D/\lambda$). Y-axis is an object density (original object density is in red—equal 0 or 1; the reconstructed density is in blue). The density threshold obtained is in green. Dark blue bars show an object shape restored by applying it to the reconstructed object density.**

sensors field, and sensors positioned at a lattice with approximately equal spacing (affected by a small random noise). The configurations tested had 4, 8, 16, 32 and 64 sensors. The object distances varied from 10 to 500 wavelengths (in physical units, it is from 0.3 to 15 m). Two types of slots, positioned to the center of the imaging field, were tested—one with walls of equal width, another with one wall twice as wide as the other. We did not add any noise to the sensor signals modeled, and assumed them exact. The object detection results presented below.

We summarize the results of detection experiments in terms of minimal object dimensions required for reliable slot detection. There are two relevant minimal dimensions for each object type—with equal and unequal walls—but it turns out that there is a difference between these types in terms of dimensions giving adequate description of reliable detection diapason. For the slot with unequal walls, relevant dimensions are the gap width and the smaller wall width. If they both exceed the values required, then the object detection is reliable. The dimensions are shown in Figs. 2 and 3.

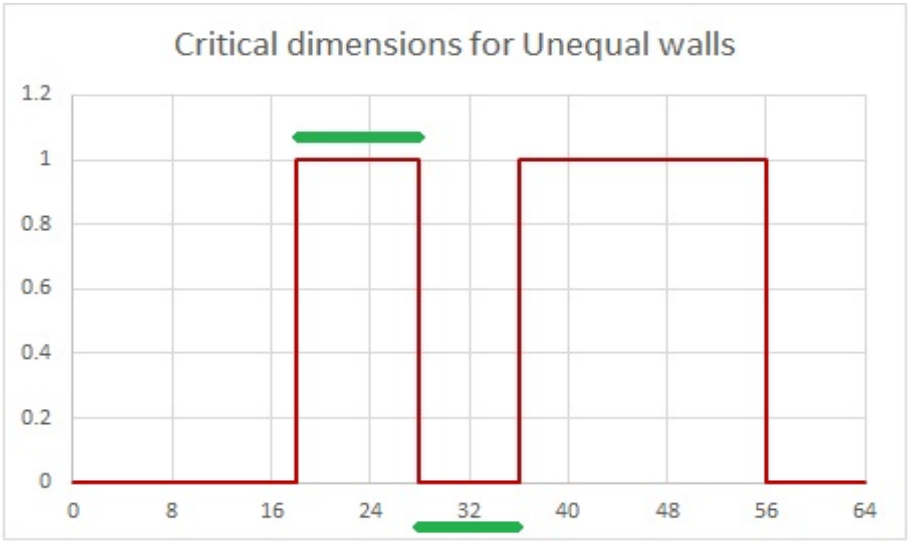


**Fig. 2 Critical dimensions for a given slot shape with unequal walls (same as above). Gap width is 8 wavelengths, and the smaller wall width is 10 wavelengths (both are shown by green bars).**

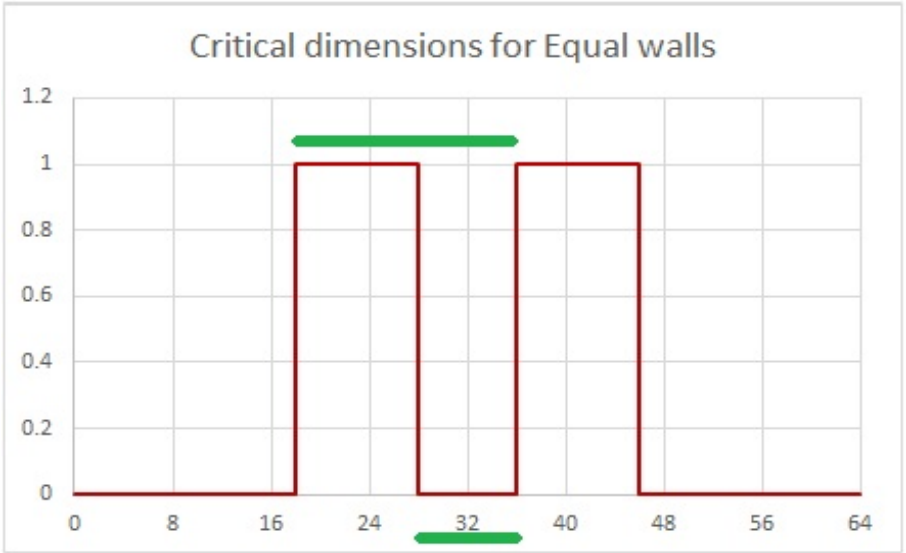


**Fig. 3 Critical dimensions for a given slot shape with equal walls. Gap width is 8 wavelengths, periodicity (the sum of wall and gap widths) is 18 wavelengths (both are shown by green arrows).**

For the slot shape with equal walls, however, the relevant dimensions are the gap width and the sum of wall width and the gap width (one may also call the latter a "periodicity parameter" of the object). If these both exceed the values required, then it turns out the object detection is reliable.

Below, we present the detection reliability data in terms of the parameters described above, for both types of objects. We give the dependency of two object's minimal required dimensions and of the detection failure rate on the distance of sensors to the object and on number of sensors used.

For the slot with unequal walls:

• Minimal gap width (in meters), depending on object distance (in meters) and number of sensors, as shown in Fig. 4;

• Minimal smaller wall width (in meters), depending on distance (in meters) and number of sensors, as shown in Fig. 5.

Here in Table 1, we may observe that detection is more reliable for distances less than 6 m and number of sensors not less than 16. The number of sensors required is in line with theoretical estimates. The spatial resolution is also best for number of sensors not less than 16 (as seen in Figs. 4 and 5 above).

It is of interest to quantify the resolution quality by introducing the quality parameter as the ratio: $\kappa = Y/r_2$, where $Y$ is given minimal critical dimension (i.e., minimal gap or wall size, etc.) and $r_2 = \sqrt{2D+1}$ is the first Fresnel zone width (from zone center to second ring boundary in zone plate) at the distance $D$. One may note that the maximal possible resolution at first Fresnel zone, $\Delta l = 1.22\Delta r_2$, equals about $0.36r_2$. Hence, we may at best obtain 0.36 as quality parameter value. Table 2 is the gap quality parameter (a ratio of a gap width to the first Fresnel zone width) values, and Table 3 shows the wall size parameter (ratio of a minimal wall width to the first Fresnel zone width).

We may see that at reliable detection zone (at 16 or more sensors), the spatial resolution for both dimensions closely approaches the minimal expected value, 0.36 of the first Fresnel zone width.

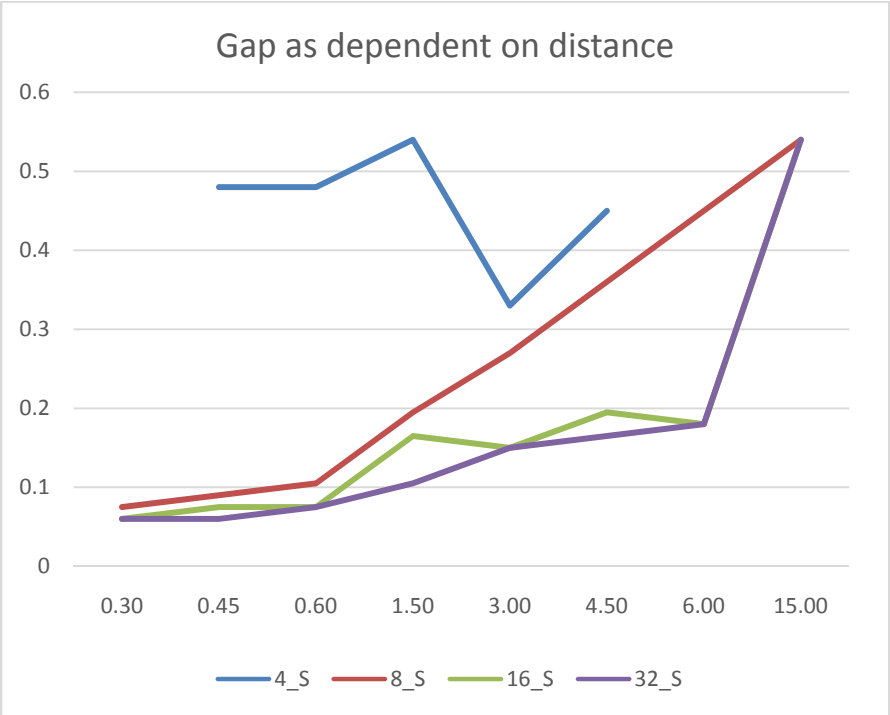


**Fig. 4 Minimal gap (in meters) required for slot shape with unequal walls for reliable detection, depending on the distance of sensors to the object (in meters). Graphs are for 4, 8, 16 and 32 sensors. The graph for 64 sensors not drawn here, as it largely coincides with the 32 sensors graph. For the four sensors, at distances of 0.3, 6 and 15 m, an algorithm fails to detect the slot.**

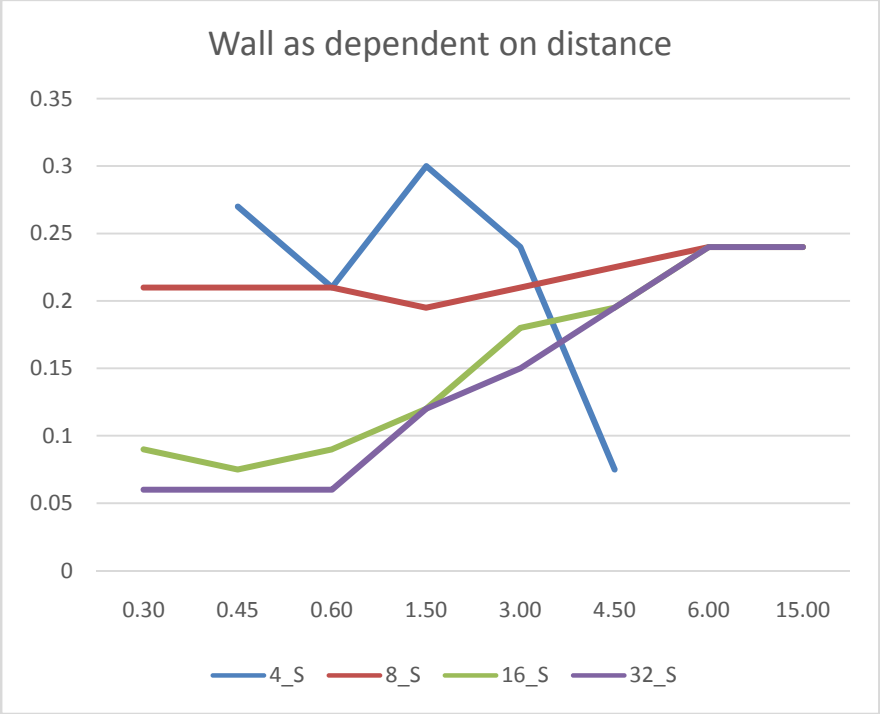


**Fig. 5 Minimal smaller wall size (in meters) required for slot shape with unequal walls for reliable detection, depending on the distance of sensors to the object (in meters). Graphs are for 4, 8, 16 and 32 sensors. The graph for 64 sensors is not drawn here, as it coincides with the 32 sensors graph.**

**Table 1 The detection failure rate for all tested slots exceeding minimal dimensions, depending on object distance (in meters) and number of sensors, for unequal walls.**

| Distance | 4_S | 8_S | 16_S | 32_S | 64_S |
|---|---|---|---|---|---|
| 0.3 | - | 18.1% | 1.7% | 0.2% | 0.0% |
| 0.45 | 13.3% | 27.4% | 5.3% | 2.6% | 2.2% |
| 0.6 | 31.4% | 4.8% | 5.1% | 4.8% | 3.4% |
| 1.5 | 0.0% | 9.7% | 1.9% | 1.3% | 2.9% |
| 3 | 24.0% | 17.6% | 4.2% | 4.3% | 3.0% |
| 4.5 | 8.3% | 16.7% | 5.6% | 6.3% | 6.3% |
| 6 | - | 30.0% | 11.6% | 9.5% | 7.4% |
| 15 | - | 20.0% | 20.0% | 53.3% | 53.3% |

**Table 2 Gap quality parameter (a ratio of a gap width to the first Fresnel zone width) values, for unequal walls.**

| Distance | 4_S | 8_S | 16_S | 32_S | 64_S |
|---|---|---|---|---|---|
| 0.3 | - | 0.55 | 0.44 | 0.44 | 0.44 |
| 0.45 | 2.87 | 0.54 | 0.45 | 0.36 | 0.36 |
| 0.6 | 2.50 | 0.55 | 0.39 | 0.39 | 0.39 |
| 1.5 | 1.79 | 0.65 | 0.55 | 0.35 | 0.35 |
| 3 | 0.78 | 0.63 | 0.35 | 0.35 | 0.46 |
| 4.5 | 0.86 | 0.69 | 0.37 | 0.32 | 0.32 |
| 6 | - | 0.75 | 0.30 | 0.30 | 0.30 |
| 15 | - | 0.57 | 0.57 | 0.57 | 0.57 |

**Table 3 Wall size parameter (ratio of a minimal wall width to the first Fresnel zone width), for unequal walls.**

| Distance | 4_S | 8_S | 16_S | 32_S | 64_S |
|---|---|---|---|---|---|
| 0.3 | - | 1.53 | 0.65 | 0.44 | 0.44 |
| 0.45 | 1.62 | 1.26 | 0.45 | 0.36 | 0.36 |
| 0.6 | 1.09 | 1.09 | 0.47 | 0.31 | 0.31 |
| 1.5 | 1.00 | 0.65 | 0.40 | 0.40 | 0.40 |
| 3 | 0.56 | 0.49 | 0.42 | 0.35 | 0.35 |
| 4.5 | 0.14 | 0.43 | 0.37 | 0.37 | 0.37 |
| 6 | - | 0.40 | 0.40 | 0.40 | 0.40 |
| 15 | - | 0.25 | 0.25 | 0.25 | 0.25 |

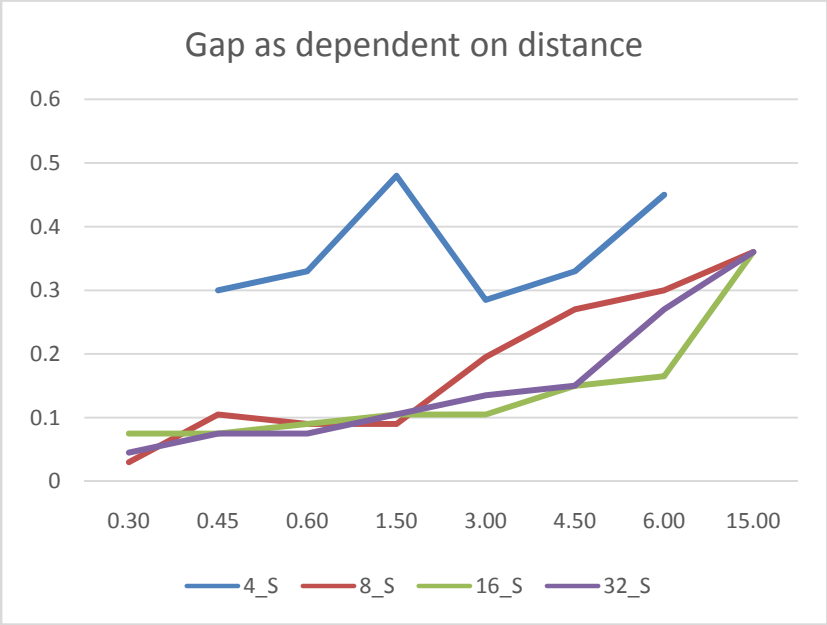


**Fig. 6 Minimal gap (in meters) required for slot shape with equal walls for reliable detection, depending on the distance of sensors to the object (in meters). Graphs are for 4, 8, 16 and 32 sensors. The graph for 64 sensors not drawn here, as it largely coincides with the 32 sensors graph. For the 4 sensors, at distances of 0.3 and 15 meters, an algorithm fails to detect the slot.**

For the slot with equal walls:

• Minimal gap width (in meters), depending on object distance (in meters) and # of sensors, shown in Fig. 6.

The same as the ratio to the first Fresnel zone width (the quality parameter) shown in Table 4.

• The other minimal dimension for that case is the sum of the widths of a wall and a gap, shown in Fig. 7.

The same as the ratio to the first Fresnel zone width (the quality parameter) shown in Table 5.

Note that the sum of sizes of two objects still does not exceed a single first Fresnel zone width.

The detection failure rate for all slots exceeding minimal dimensions, depending on object distance (in meters) and number of sensors, shown in Table 6.

We see that for slots of that type, detection is reliable at distances up to 15 m, with number of sensors not less than 16. With eight sensors, detection reliability and resolution are weaker.

**Table 4 Gap quality parameter (a ratio of a gap width to the first Fresnel zone width) values, for equal walls.**

| Distance | 4_S | 8_S | 16_S | 32_S | 64_S |
|---|---|---|---|---|---|
| 0.3 | - | 0.22 | 0.55 | 0.33 | 0.44 |
| 0.45 | 1.80 | 0.63 | 0.45 | 0.45 | 0.45 |
| 0.6 | 1.72 | 0.47 | 0.47 | 0.39 | 0.39 |
| 1.5 | 1.59 | 0.30 | 0.35 | 0.35 | 0.35 |
| 3 | 0.67 | 0.46 | 0.25 | 0.32 | 0.21 |
| 4.5 | 0.63 | 0.52 | 0.29 | 0.29 | 0.29 |
| 6 | 0.75 | 0.50 | 0.27 | 0.45 | 0.45 |
| 15 | - | 0.38 | 0.38 | 0.38 | 0.38 |

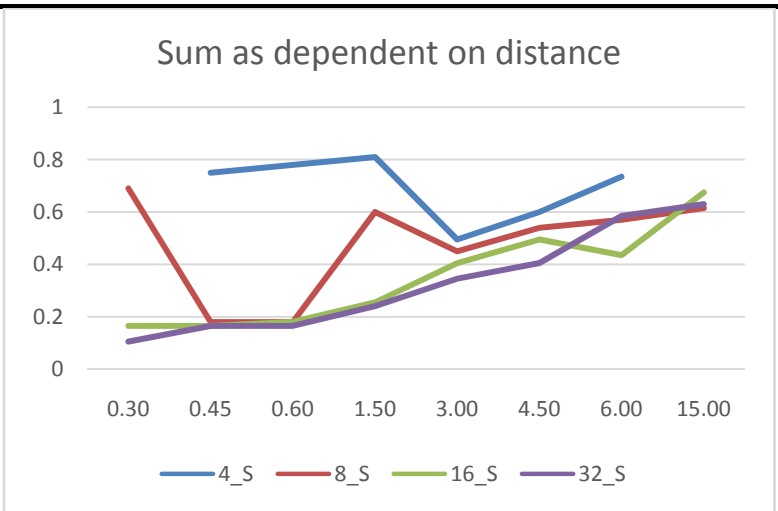


**Fig. 7 The minimal sum of wall size and the gap (in meters) required for slot shape with equal walls for reliable detection, depending on the distance of sensors to the object (in meters). Graphs are for 4, 8, 16 and 32 sensors. The graph for 64 sensors is not drawn here, as it largely coincides with the 32 sensors graph.**

**Table 5 Sum quality parameter (a ratio of a sum of wall size and the gap to the first Fresnel zone width), for equal walls.**

| Distance | 4_S | 8_S | 16_S | 32_S | 64_S |
|---|---|---|---|---|---|
| 0.3 | - | 5.02 | 1.20 | 0.76 | 1.09 |
| 0.45 | 4.49 | 1.08 | 0.99 | 0.99 | 0.99 |
| 0.6 | 4.06 | 0.94 | 0.94 | 0.86 | 0.86 |
| 1.5 | 2.69 | 1.99 | 0.85 | 0.80 | 0.80 |
| 3 | 1.16 | 1.06 | 0.95 | 0.81 | 0.81 |
| 4.5 | 1.15 | 1.04 | 0.95 | 0.78 | 0.78 |
| 6 | 1.22 | 0.95 | 0.72 | 0.97 | 1.00 |
| 15 | - | 0.65 | 0.71 | 0.66 | 0.70 |

**Table 6 The detection failure rate for all slots exceeding minimal dimensions, depending on object distance (in meters) and number of sensors, for equal walls.**

| Distance | 4_S | 8_S | 16_S | 32_S | 64_S |
|---|---|---|---|---|---|
| 0.3 | - | 3.1% | 0.0% | 0.0% | 0.4% |
| 0.45 | 2.8% | 2.2% | 0.2% | 0.2% | 0.2% |
| 0.6 | 8.0% | 1.7% | 0.2% | 0.4% | 0.4% |
| 1.5 | 37.5% | 1.1% | 0.0% | 0.7% | 0.5% |
| 3 | 3.6% | 3.9% | 1.0% | 0.9% | 3.3% |
| 4.5 | 6.6% | 4.3% | 0.5% | 1.1% | 2.8% |
| 6 | 0.0% | 5.3% | 4.8% | 0.0% | 1.1% |
| 15 | - | 6.2% | 0.0% | 0.0% | 0.0% |

## 5. Conclusions

In this work, we presented, by combining the well-known building blocks (generalized Fourier-basis deconvolution, a specific type of Tikhonov regularization in Hermitian space, and a threshold-based object detection technique), a concrete version of microwave holographic imaging and obstacle detection algorithm for an environment with a single coherent emitter and few detection sensors. The version is computationally efficient, requiring just $O(N*K)$ operations per image frame, where $K$ is the number of signals detected (sensors) and $N$ is the number of image elements (pixels). There exist wide varieties of signal processing approaches with the given algorithm, defined by the choice of functional space and a regularization metrics, allowing for adaptive treatment of sensor data based on the output of the other parts of the collaborative object recognition system. The algorithm suggested would offer, even in its simple form, a reliable object detection with spatial resolution matching the a priori theoretical expectations for a model 1D task of slot detection. The detection distances and spatial resolution achieved (better than 20 cm on distances up to 4.5 m) are sufficient for near-vehicle object detection purposes. An important direction for future research is to focus on distance measurement precision with object detection algorithms (the experiments presented in this article concentrated on a width measurement task only). The numerical experiments on 2D and 3D shapes detection, systematic treatment for signal noise effects, and the testing with the actual physical objects all are the subject for the future work.

## Acknowledgments

We gratefully acknowledge the support from the Russian Science Foundation, project number 16-19-00181, for this work.

## References

[1] Safercar.gov. n.d. Automatic Emergency Braking. Accessed December 7, 2017. https://www.safercar.gov/Vehicle-Shoppers/Safety-Technology/aeb%E2%80%931.

[2] Fu, L., Gui, Y. S., Bai, L. H., Guo, H., Abou-Rachid, H., and Hu, C.-M. 2015. "Microwave Holography Using a Magnetic Tunnel Junction Based Spintronic Microwave Sensor." *Journal of Applied Physics* 117: 213902.

[3] Miwa, S., Ishibashi, S., Tomita, H., Nozaki, T., Tamura, E., Ando, K., et al. 2014. "Highly Sensitive Nanoscale Spin-Torque Diode." *Nature Materials* 13: 50-6.

[4] Goodman, J. W., and Lawrence, R. W. 1967. "Digital Image Formation from Electronically Detected Holograms." *Appl. Phys. Lett.* 11: 77-9.

[5] Huang, T. 1971. "Digital Holography." *Proc. IEEE* 59: 1335-46.

[6] Schnars, U. 1994. "Direct Phase Determination in Hologram Interferometry with Use of Digitally Recorded Holograms." *J. Opt. Soc. Am. A* 11: 2011-5.

[7] Okano, F., Hoshino, H., Arai, J., and Yuyama, I. 1997. "Real-Time Pickup Method for a Three-Dimensional Image Based on Integral Photography." Applied Optics 36 (7): 1598-603.

[8] Okano, F., Arai, J., Hoshino, H., and Yuyama, I. 1999. "Three-Dimensional Video System Based on Integral Photography." *Optical Engineering* 38 (6): 1072-7.

[9] Yamaguchi, I., and Zhang, T. "Phase-Shifting Digital Holography." *Opt. Lett.* 22: 1268-70.

[10] Takaki, Y., and Ohzu, H. 1999. "Fast Numerical Reconstruction Technique for High-Resolution Hybrid Holographic Microscopy." *Appl. Opt.* 38: 2204-11.

[11] Cuche, E., Marquet, P., and Depeursinge, C. 2000. "Spatial Filtering for Zero-Order and Twin-Image Elimination in Digital Off-Axis Holography." *Appl. Opt.* 39: 4070-5.

[12] Arimoto, H., and Javidi, B. 2001. "Integral Three-Dimensional Imaging with Digital Reconstruction." *Optics Letters* 26 (3): 157-9.

[13] Frauel, Y., Tajahuerce, E., Matoba, O., Castro, A., and Javidi, B. 2004. "Comparison of Passive Ranging Integral Imaging and Active Imaging Digital Holography for Three-Dimensional Object Recognition." *Applied Optics* 43 (2): 452-2.

[14] Xu, W., Jericho, M. H., Meinertzhagen, I. A., and Kreuzer, H. J. 2001. "Digital In-line Holography for Biological Applications." *Proc. Natl. Acad. Sci.* 98: 11301-5.

[15] Zhang, Y. 2003. "Whole Optical Wave Field Reconstruction from Double or Multi In-line Holograms by Phase Retrieval Algorithm." *Optics Express* 11 (24): 3234-41.

[16] Repetto, L., Piano, E., and Pontiggia, C. 2004. "Lensless Digital Holographic Microscope with Light-Emitting Diode Illumination." *Opt. Lett.* 29: 1132-4.

[17] Kreis, T. 2005. *Handbook of Holographic Interferometry: Optical and Digital Methods.* Weinheim: Wiley-VCH Verlag GmbH & Co. KGaA.

[18] Pedrini, G., Osten, W., and Zhang, Y. 2005. "Wave-Front Reconstruction from a Sequence of Interferograms Recorded at Different Planes." *Opt. Lett.* 30: 833-5.

[19] Kalenkov, G. S., Kalenkov, S. G., and Shtan'Ko, A. E. 2015. "Hyperspectral Holographic Fourier-Microscopy." *Quantum Electronics* 45 (4): 333-8.

[20] Holl, P. M., and Reinhard, F. 2017. "Holography of Wi-Fi Radiation." *Phys. Rev. Lett.* 118: 183901.

[21] Benedetti, M., Donelli, M., Martini, A., Pastorino, M., Rosani, A., and Massa, A. 2006. "An Innovative Microwave-Imaging Technique for Nondestructive Evaluation: Applications to Civil Structures Monitoring and Biological Bodies Inspection." *IEEE Trans. Instrum. Meas.* 55: 1878-84.

[22] Tsihrintziz, G. A., and Devaney, A. J. 2000. "Higher-Order (Nonlinear) Diffraction Tomography: Reconstruction Algorithms and Computer Simulation." *IEEE Trans. Image Process.* 9: 1560-72.

[23] Charrière, F., Colomb, T., Depeursinge, C., Marquet, P., and Cuche, E. 2006. "Digital Holographic Microscopy Applied to Diffraction Tomography of a Cell Refractive Index." *Optics Letters* 31 (2): 178-80.

[24] Sung, Y., Choi, W., Fang-Yen, C., Badizadegan, K., Dasari, R., and Feld, M. 2009. "Optical Diffraction Tomography for High Resolution Live Cell Imaging." *Optics Express* 17 (1): 266-77.

[25] Kotelnikov, V. A. 1993. "On the Carrying Capacity of the Ether and Wire in Telecommunications." Presented at Material for the First All-Union Conference on Questions of Communication, Izd. Red. Upr. Svyazi RKKA 1933, Moscow. (in Russian)

[26] Whittaker, E. T. 1915. "On the Functions Which Are Represented by the Expansions of the Interpolation Theory." *Proc. Royal Soc.* 35: 181-94.

[27] Nyquist, H. 1928. "Certain Topics in Telegraph Transmission Theory." *Trans. AIEE* 47: 617-44.

[28] Shannon, C. E. 1948. "A Mathematical Theory of Communication." *Bell System Technical Journal* 27 (3): 379-423.

[29] Tikhonov, A. N. 1943. "On the Stability of Inverse Problems (in Russian)." *Doklady Akademii Nauk SSSR* 39 (5): 195-8.

[30] Tikhonov, A. N. 1963. "Solution of Incorrectly Formulated Problems and the Regularization Method." *Soviet Mathematics* 4: 1035-8.

[31] Tikhonov, A. N., and Arsenin V. Y. 1977. *Solution of Ill-Posed Problems.* Washington: Winston & Sons.

[32] Tikhonov, A. N., Goncharsky, A. V., Stepanov, V. V., and Yagola, A. G. 1995. *Numerical Methods for the Solution of Ill-Posed Problems.* Dordrecht, the Netherlands: Kluwer Academic Publishers.